TECHNICAL ARTICLE

Bubble Formation and Surface Sloshing in the TSL Flow with a Viscous Liquid

LINGLING CAO,[1] YANNAN WANG,[2,4] ZHONGFU CHENG,[3] HONGMING WANG,[1] and GUIRONG LI[1]

1.—School of Materials Science and Engineering, Jiangsu University, Zhenjiang 212013, China. 2.—School of Energy and Power Engineering, Jiangsu University, Zhenjiang 212013, China. 3.—Department of Materials Engineering, KU Leuven, 3000 Leuven, Belgium. 4.—e-mail: yannan.wang@ujs.edu.cn

Due to the ever-increasing importance of the top-submerged lance (TSL) process in metal recycling and slag valorization, considerable effort have been devoted to studying TSL flow characteristics. In this work, the bubble formation and surface sloshing in a TSL flow with a viscous liquid are numerically investigated by the volume-of-fluid model coupled with large eddy simulation approach. First, the numerical model is validated by high-resolution particle imaging velocimetry (HR-PIV) experiments in both qualitative and quantitative manners. After that, the numerical model is adopted to determine the bubbling frequencies at various operational conditions. The results show that the bubbling frequency decreases with increasing gas flow rate, and it slightly depends on the lance submergence depth. Besides, a dimensionless correlation is proposed considering inertial force, viscous force and surface tension. Similar correlations are achieved for the present work and the experimental work from the literature. The agreement highlights the ability of the proposed correlation to evaluate bubbling frequency obtained at diverse conditions. In addition, the influences of gas flow rate and lance submergence depth on surface sloshing behavior are clarified. This fundamental work gives insights into the TSL flow physics, the understanding of which can aid in TSL process control and optimization.

INTRODUCTION

Top-submerged gas injection technology is gaining great popularity in processing different kinds of secondary resources, e.g., recycling precious metals from waste electric and electronic equipment (WEEE),[1,2] extracting nonferrous metals from waste metallurgical slags or residues,[3–6] and valorizing metallurgical slags towards high-added value construct products.[7–10] Due to the high flexibility and high recovery rate of top-submerged lance (TSL) technology such as Ausmelt and Isasmelt technology, it has been categorized as one of the best available techniques (BAT).[11] The increasing importance of TSL technology in practice attracts considerable efforts from both the industrial and academic communities to investigate the flow characteristics in a reactor bath, e.g., the bubble behavior and surface sloshing, which have crucial influences on process control and optimization. However, due to the difficulties of high-temperature experiments (e.g., opacity of a TSL reactor, hazardous operating environment, lack of measuring techniques at high temperature), two approaches, i.e., low temperature physical modeling[12,13] and numerical simulation,[14–16] are usually adopted to study the gas–liquid two-phase flow physics in the TSL bath.

Considering the correlation between bubble formation and pressure fluctuation in lance, Gosset et al.[12] experimentally investigated the effects of gas flow rate and lance submergence depth on the bubbling frequency by monitoring pressure signals at the top of the lance in a helium/air–water system. It was found that the bubbling frequency remains

almost constant with the helium gas flow rate < 1.5 L/s, increases to a local maximum at 3.5 L/s, and then decreases as the helium gas flow rate continues increasing. The obtained bubbling frequency ranged between 6 to 12 Hz, which was consistent with the findings by Neven.[17] It was also noticed that the bubbly frequency slightly increases with decreasing lance submergence depth. This was explained by the interaction between bath surface motion and gas bubble, which resulted in a premature detachment of gas bubbles and thus a higher bubbling frequency. Moreover, to quantify the bubbling frequency at various operational conditions, Gosset et al. proposed a dimensionless correlation between the Strouhal number (St) and the ratio of the Weber number to the Bond number (We/Bo), as seen in St = 0.00126(We/Bo)$^{-0.61}$. Akashi et al.[13] experimentally studied the bubble formation by using x-ray radiography and high-speed imaging in a argon-liquid metal system. They found that the bubbling frequency slightly decreases with increasing gas flow rate at the middle and top lance position, while the bubbling frequency exhibits small variation with gas flow rate at the bottom lance position. As the lance submergence depth increases, the bubbling frequency linearly increases. This is inconsistent with the finding by Gosset et al. as described above. In addition, a similar dimensionless correlation was obtained by Akashi et al. with deviation in the pre-exponential factor and exponent. The deviation is considered to be caused by the differences in material properties, especially the surface tension. Besides, the confinement effect generated by the quasi-2D vessel can also have a large impact on the bubble formation. Recently, Kandalam et al.[18] performed acoustic and lance motion measurements to study bubbly dynamics in an air–water system. By processing the acoustic signals and the data obtained by a motion sensor, the bubble collapse frequency and bubble detachment frequency were determined respectively. These techniques are expected to be successfully applied into industrial case. The aforementioned work focuses on the bubble formation in a less viscous liquid such as water and liquid metal. It may be misleading to apply the results to optimizing the industrial processes with viscous liquids such as the metal-containing metallurgical slags or residues. To overcome this issue, studies were performed on gas-viscous liquid systems, e.g., air-paraffin oil system,[14] air-glycerol system,[19] and air-molten slag system.[20,21] However, the bubbling frequency in these studies was reported at a given operating condition, and no detailed parametric study was included to evaluate the influences of operational parameters (e.g., gas flow rate, lance submergence depth) on the bubble formation. Bubble frequency ranging from 2.5 Hz to 20 Hz was measured by processing the pressure signals or the gas volume fraction. With limited data of bubble frequency and large differences in material properties (e.g.,

density, viscosity, surface tension) from the few studies, it is difficult to understand the bubble formation behavior in viscous liquids.

Regarding to the bath sloshing behavior in TSL flows, only few studies have been performed.[15,16,20–22] Liow et al.[22] experimentally investigated the sloshing behavior of a TSL flow in an air–water system. It was observed that the amplitude of the sloshing wave initially increases with the lance submergence depth and then decreases after reaching a maximum. The amplitude of the sloshing wave monotonically increased with increasing gas flow rate to a maximum and then drops to an almost constant value. In addition, the sloshing wave suddenly disappeared at a flow rate of 1.5 L/s. The disappearance of sloshing wave was also noted in a water modeling of the Pierce-Smith converter.[23] Wang et al.[20] numerically investigated the surface sloshing in a gas-molten slag system. By tracking and processing the volume fraction of gas/liquid phase, it was found that the amplitude of the sloshing wave increases with increasing lance submergence depth, whereas the wave frequency remains constant. Applying the same numerical method into a gas–liquid metal system, Obiso et al.[15] found an oscillatory sloshing wave with a frequency of 2 Hz present at the top lance position and no sloshing wave at the bottom lance position. This finding indicated that the presence of a sloshing wave depends on the lance submerged depth. Subsequently, Obiso et al.[16] studied the sloshing behavior of this gas–liquid metal system in a 3D cylindrical vessel. It was revealed the rotational sloshing is maintained by the synchronism between gas bubbles and bath surface. Through specific post-processing of the simulation results, this synchronism phenomenon can be vividly observed. Moreover, they also investigated the sloshing behavior of a slag bath in a pilot-scale TSL furnace.[21] The wave frequencies were 1.217 Hz and 1.199 Hz for a non-swirling configuration and a swirling configuration, which were approximately equal to half of the bubbling frequencies. The obtained results agreed with the experimental data measured by Player for an industrial Isasmelt process.[24] The mentioned studies by Obiso et al. help to understand TSL flow phenomena in detail, which can aid in the overall optimization of TSL flow. In addition, Huda et al.[25] studied zinc fuming behavior by CFD modeling. It was found that the fuming rate increases when the lance submergence depth increases. It was explained that increasing lance submergence depth leads to a noteworthy increment in sloshing and splash generation. However, no quantitative description was shown on surface sloshing. The effect of surface sloshing behavior on chemical reactions in practical case needs to be investigated in future work.

Even though a number of studies have been performed on bubble formation and surface sloshing in TSL flows, two aspects still need to be addressed: (1) To better represent the flow characteristics of

industrial TSL process, more studies on bubble formation and sloshing behavior in viscous liquids are necessary, especially a study focusing on the effects of different operating conditions. (2) A comparison study is necessary to clarify the effects of viscosity and surface tension. In this work, a numerical approach, i.e., volume-of-fluid (VOF) model coupled with large eddy simulation (LES), is adopted to study the key features, namely, bubble formation and surface sloshing behavior in a viscous liquid. Compared to the less viscous liquids such as water and liquid metal frequently used in previous studies, a detailed study on the viscous liquid can provide a better understanding of the practical TSL flows involving viscous slags and residues.

EXPERIMENTAL AND NUMERICAL METHODOLOGY

Experimental Setup

To validate the numerical model used in this work, high-resolution particle imaging velocimetry (HR-PIV) experiments are conducted in an air-paraffin oil two-phase system. Air and paraffin oil are used to simulate the gas and viscous slag phase in the slag valorization and metal recycling process. The HR-PIV experimental setup is given in Fig. 1. The vessel has dimensions of 0.135 m × 0.135 m × 0.195 m. The outer and inner diameters of the lance are 0.008 m and 0.005 m. The geometrical information and materials properties are listed in Table S1 (see Supplementary Material). Considering the maximal pixel displacement, the relative error of the instantaneous velocity measured by the PIV experiment is < 2%. The sampling error on the mean velocity is estimated to be < 2% based on the sampling size of 1024. Therefore, the total relative error is < 5%. The detailed experimental procedures can be found in the work of Wang et al.[14] and Vanierschot et al.;[26] therefore, it will not be repeated here. It is worth mentioning that a square vessel was used in the PIV experiments for the convenience of data collection. This is different with practical cases where circular vessels are usually used as reactors. The difference associated with

vessel shape is likely to cause deviation of flow pattern from industrial cases. In addition, the effect of the vessel shape on bubbling frequency and surface sloshing wave has not been clarified. This needs to be further studied in future. For the measured zone in Fig. 1b, it was chosen to avoid the interference from rising gas bubbles, which can severely deteriorate the fidelity of the experimental data.

Numerical Approach

The numerical simulations are performed with the commercial software package ANSYS FLUENT 2021R1. The VOF model is used to simulate the two-phase flow, given that the advanced interface-tracking algorithm, i.e., geometric reconstruction scheme developed by Youngs,[27] is incorporated in this model, which makes it perfectly suitable to resolve the bubble formation and wave propagation behavior. In the VOF model variables are shared with all phases. Therefore, only one set of the mass and momentum conservation equations is solved in Eqs. 1 and 2. The surface tension force, as a source term in the momentum conservation equation, is simulated based on the continuum surface force (CSF) model developed by Brackbill et al.[28] The LES model is used to resolve the turbulence in the TSL flow. Among various sub-grid scale (SGS) models in LES, the Dynamic Smagorinsky-Lilly (DSL) model is adopted to compute the eddy viscosity, during which the model constant can be dynamically determined instead of a priori constant value.[29,30] With this merit the DSL model is expected to be more accurate in predicting the turbulent quantities. The operational parameters for all simulations are displayed in Table I. The dimensionless numbers, i.e., the modified Froude number, Fr_m, the Reynolds number, Re, the Bond number, Bo, and the Weber number, We, are calculated to describe the TSL flow, as seen in Eqs. 3–6.

$$\frac{\partial}{\partial t}(\rho\alpha) + \nabla \cdot (\rho\alpha\vec{u}) = 0 \tag{1}$$

$$\frac{\partial}{\partial t}(\rho\vec{u}) + \nabla \cdot (\rho\vec{u}\vec{u}) = -\nabla p + \nabla \cdot \vec{\tau} + \rho\vec{g} + \vec{F}_{\text{csf}} \tag{2}$$

where ρ is density, kg/m^3; α is phase volume fraction; u is velocity, m/s; p is pressure, Pa; τ is stress tensor, N/m^2; g is the gravitational acceleration, m/s^2; F_{csf} is surface tension force, N/m^2.

$$\text{Fr}_m = \frac{\rho_g u_g^2}{(\rho_l - \rho_g)g d_{\text{in}}} \tag{3}$$

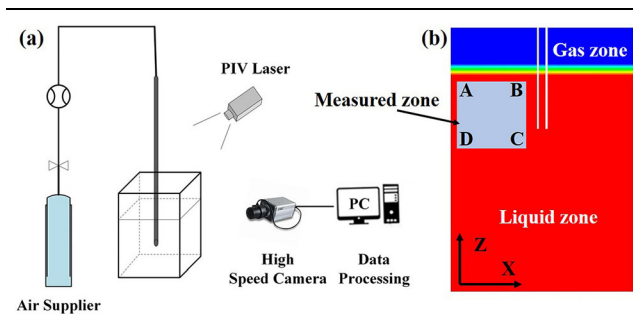$$\text{Re} = \frac{\rho_g u_g d_{\text{in}}}{\mu_g} \tag{4}$$

Fig. 1. (a) HR-PIV setup and (b) PIV measured zone 0.058 m × 0.058 m: A (− 0.065, 0, 0.164); B (− 0.007, 0, 0.164); C (− 0.007, 0, 0.106); D (− 0.065, 0, 0.106).

Table I. Operational parameters used in all simulations

Case	Gas flow rate, L/s	Lance submergence depth, m	Fr_m	Re	Bo	We
L44FLR350*	0.097	0.044	0.70	1700	8.28	5.78
L44FLR500	0.139	0.044	1.42	2420	8.28	11.80
L44FLR800	0.222	0.044	3.63	3870	8.28	30.10
L44FLR1240	0.344	0.044	8.76	6010	8.28	72.56
L44FLR1600	0.444	0.044	14.59	7750	8.28	120.86
L44FLR2400	0.667	0.044	32.89	11,600	8.28	272.33
L88FLR350*	0.097	0.088	0.70	1700	8.28	5.78
L110FLR350	0.097	0.110	0.70	1700	8.28	5.78

"*"Indicates the cases for validation.

$$Bo = \frac{(\rho_l - \rho_g)gd_{in}^2}{\sigma} \quad (5)$$

$$We = \frac{\rho_g d_{in} u_g^2}{\sigma} \quad (6)$$

where d_{in} is the inner diameter of lance, m; μ is viscosity, kg/(m s); σ is surface tension, N/m; subscripts, i.e., g and l, indicate the gas and liquid phase.

Numerical Setup

Structured meshes are generated by using ICEM software. Based on the grid independence study in our previous work,[14] grid number of approximately 350,000 is sufficient for the simulation, resulting in a range of 0.3–4.0 mm for the grid size. The velocity inlet and pressure outlet are used as the boundary condition in the simulations. The Semi-Implicit Method for Pressure-Linked Equations-Consistent (SIMPLEC) scheme[31] is adopted to solve the velocity–pressure coupling equation. The PREssure STaggering Option (PRESTO!) and bounded central differencing schemes are used to discretize the pressure and momentum equations. In the simulations, the convergence criterion is set as 1×10^{-6}, and the residual of the continuity equation drops at least three orders of magnitude before meeting the convergence criterion. For all simulations, the maximum Courant number is kept below 1.0, leading to the time step in the order of magnitude of 10^{-5} s.

RESULTS AND DISCUSSION

Model Validation

To obtain high-fidelity data from the simulations, the numerical model is validated by the HR-PIV experimental data. As noted in Table I, two cases, i.e., L44FLR350 and L88FLR350, are used for the validation. Figure 2 shows the flow patterns obtained from the PIV experiments and simulations. It can be found that numerical results

qualitatively agree with the experimental data, as the main recirculation and the velocity gradient from the near lance region to the near wall region are captured in both cases. As two main flow features in this TSL flow, the recirculation and the velocity gradient are caused by the rising gas bubbles, which drive the viscous liquid to move in this pattern. Figure 3 presents the experimental and numerical velocity fields, where a large velocity region near the submerged lance is predicted by the simulation. The numerical velocity is dissipated from the bubbly zone to the near wall region, generating a large velocity gradient, which is consistent with the experimental observation. However, a large discrepancy in the maximum velocity magnitude is also noticed. Approximately 0.67 m/s of the velocity magnitude is obtained in the simulation of L44FLR350 case (see Fig. 3b), while around 0.27 m/s is measured in PIV experiment (see Fig. 3a). For the L88FLR350 case, approximately 0.52 m/s of the velocity magnitude is obtained (see Fig. 3e), while around 0.33 m/s in experiment (see Fig. 3d). The discrepancy is mainly due to the numerical procedure in VOF model, where the velocity is phase averaged. Since the gas velocity is much larger than the liquid velocity, this results in an over-predicting phase-averaged velocity compared to the pure liquid velocity in PIV experiment. Another factor for the discrepancy is the experimental error caused by the refraction of gas bubbles. To solve this deviation, a filtering method proposed by Obiso et al.[32] is used to reduce the negative influence of the presence of gas phase on the prediction of velocity magnitude. As shown in Fig. 3c and f, the maximum velocity magnitudes for L44FLR350 and L88FLR350 cases are decreased to around 0.38 m/s and 0.34 m/s, which become closer to the maximum values in experiments.

To have a quantitative validation between experiment and simulation, the data along the recirculation center are extracted and compared, during which the aforementioned filtering method is used. Figure 4 shows that good agreement is achieved in most of the regions; however, deviations exist in the
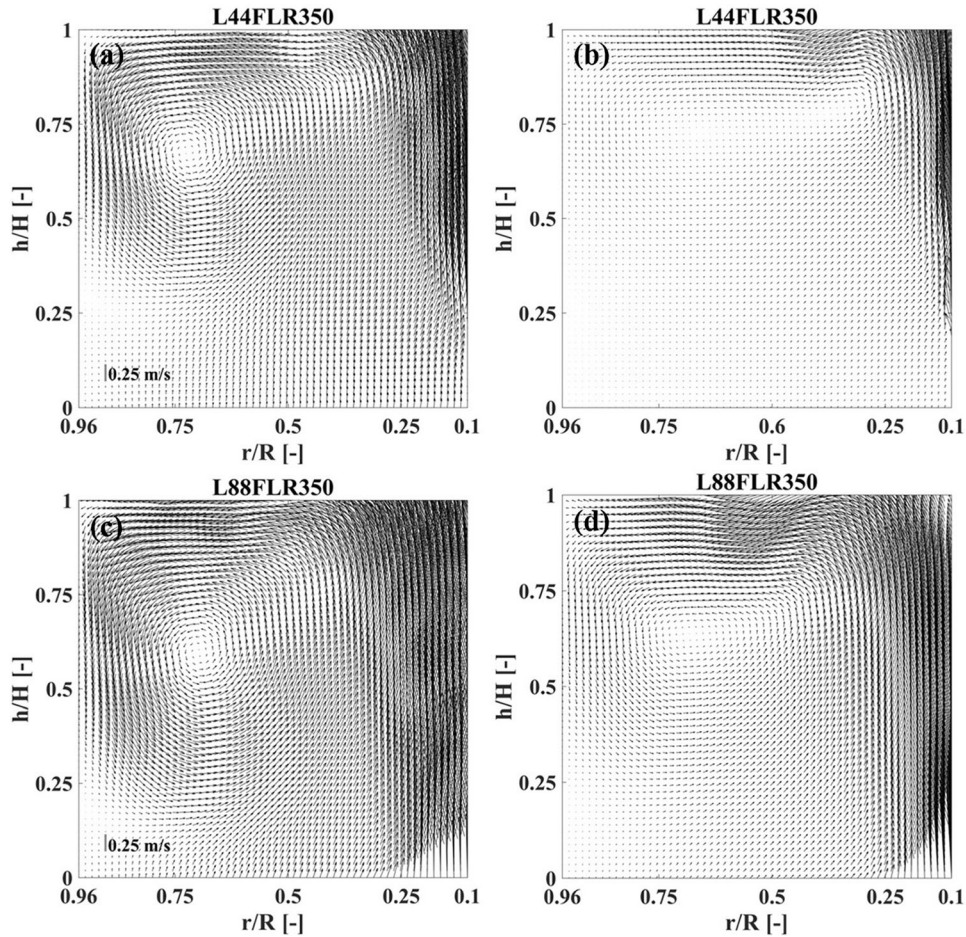
Fig. 2. Experimental and numerical flow patterns for L44FLR350 and L88FLR350 (a) and (c) experimental; (b) and (d) LES-DSL model (r: radial distance from the axial line; R: radial distance between the axial line and wall; h: axial distance from the bottom of the measured zone; H: height of the measured zone).

near lance region and the near wall region. In general, consistency is obtained between the experiment and simulation for both cases. Figure 5 shows the comparison of the velocity fluctuations which are obtained by calculating the root-mean-square (RMS) values of the instantaneous velocities. Clearly, a large overestimation by the simulation is observed in the near lance region (approximately $r/R < 0.25$). Since gas bubbles are concentrated in the near lance region, this may cause the failure of the DSL model. It indicates that the disturbance of the gas phase on flow turbulence needs to be taken into account in the DSL model, which is a single-phase turbulence model. In the rest region, the velocity fluctuations are captured by the DSL model for both cases. Based on the above comparisons, the numerical model, i.e., VOF-LES-DSL has been corroborated.

Bubble Formation

After the numerical model being validated, it is used to study the bubble formation in the viscous liquid. The pressure signals are tracked in two

positions with the coordinates of (0 m, 0 m, 0.16 m) and (0 m, 0 m, 0.145 m) in the lance. By averaging the pressure signals and processing them with a fast Fourier transform (FFT) technique, the bubbling frequencies are obtained at various operational conditions. Figure 6 shows the pressure signals and bubbling frequencies for L44FLR350 and L44FLR1250 cases to illustrate this method. Figure 6a and c shows that the pressure varies periodically, suggesting a constant frequency of bubble formation and detachment. This bubbling frequency is determined by applying the Gaussian function with nonlinear Marquardt–Levenberg algorithm to the FFT spectrum, as seen in Fig. 6b and d. The relationship between bubbling frequency and gas flow rate is depicted in Fig. 7a, which demonstrates that the bubbling frequency decreases with increasing gas flow rate. This finding is consistent with the work of Akashi et al.,[13] where bubbling frequency was experimentally measured by x-ray radiography and high-speed camera in an argon-liquid metal system. The influence of lance submergence depth on the bubbling frequency has been investigated as well. The results displayed in
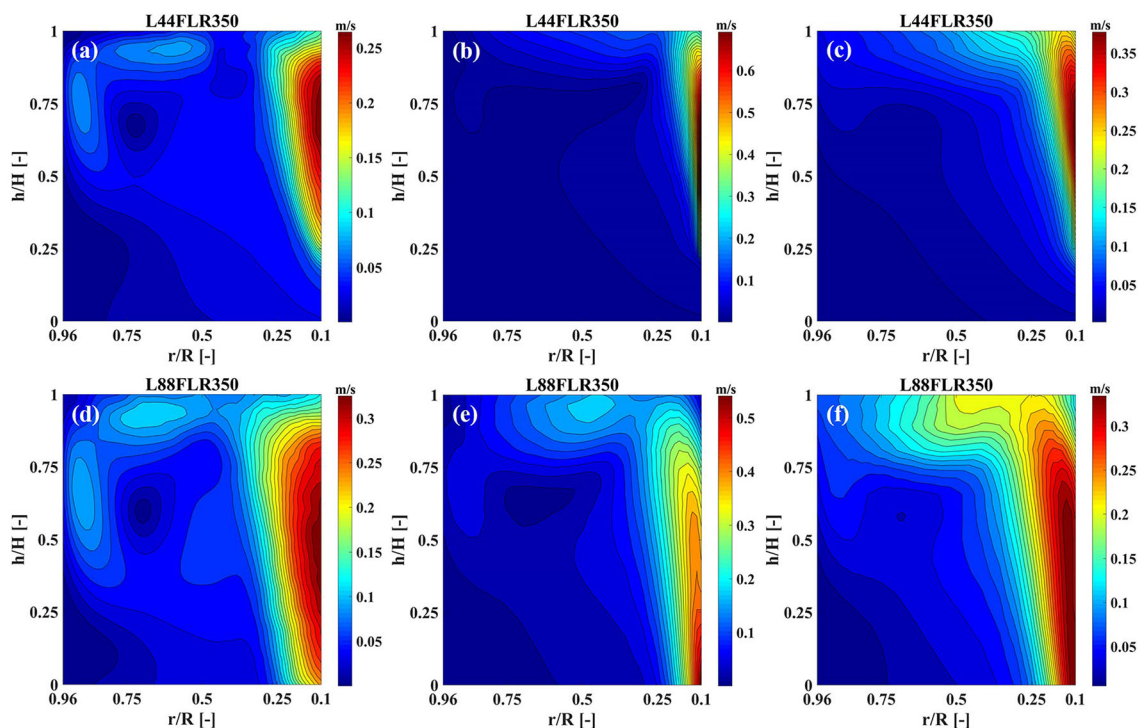
Fig. 3. Experimental and numerical velocity fields (a) and (d) experimental; (b) and (e) LES-DSL without filtering method; (c) and (f) LES-DSL with filtering method (r: radial distance from the axial line; R: radial distance between the axial line and wall; h: axial distance from the bottom of the measured zone; H: height of the measured zone).

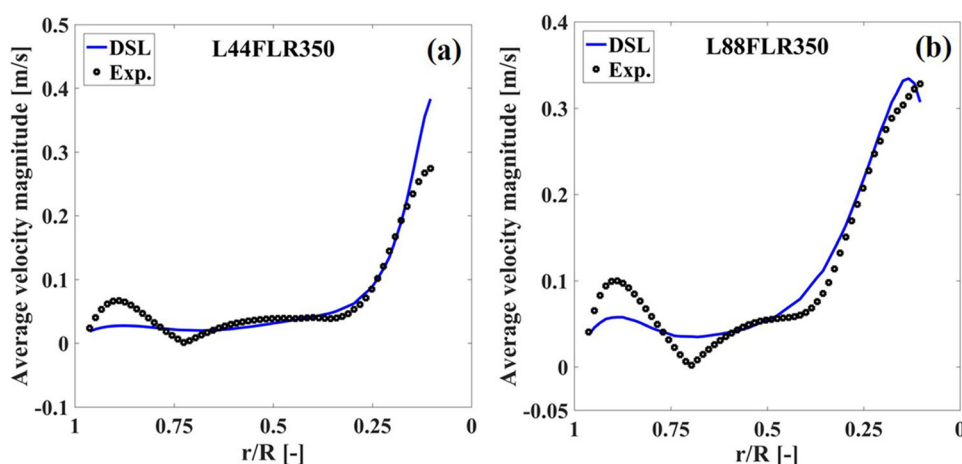Fig. 4. Average velocity magnitude along the line through the recirculation center: (a) L44FLR350; (b) L88FLR350 (r: radial distance from the axial line; R: radial distance between the axial line and wall).

Fig. 7b reveal that the bubbling frequency changes slightly, approximately 5%, as the lance submergence depth ranges from 0.044 m to 0.11 m. It appears that the lance submergence depth has limited influence on the bubbly frequency in this gas-viscous liquid system. This finding has been confirmed in less viscous systems. In the argon-liquid metal system by Akashi et al.,[13] the mean bubbling frequency varied by around 15% with the lance submergence depth. Moreover, in the helium-water system by Neven,[17] no significant change of bubbling frequency was observed with lance submergence depth. However, only three data points were collected in the present; a detailed investigation is necessary to further verify this conclusion.

In the present wok, bubbling frequency with a range of 12.5–19 Hz has been detected, which is higher than the bubbling frequency of 7–12 Hz in the work of Gosset et al.[12] and 10–14 Hz in the work of Akashi et al.[13] The difference can be attributed to the distinct physical properties of the materials and diverse operational conditions in the work. The information of operational systems and conditions
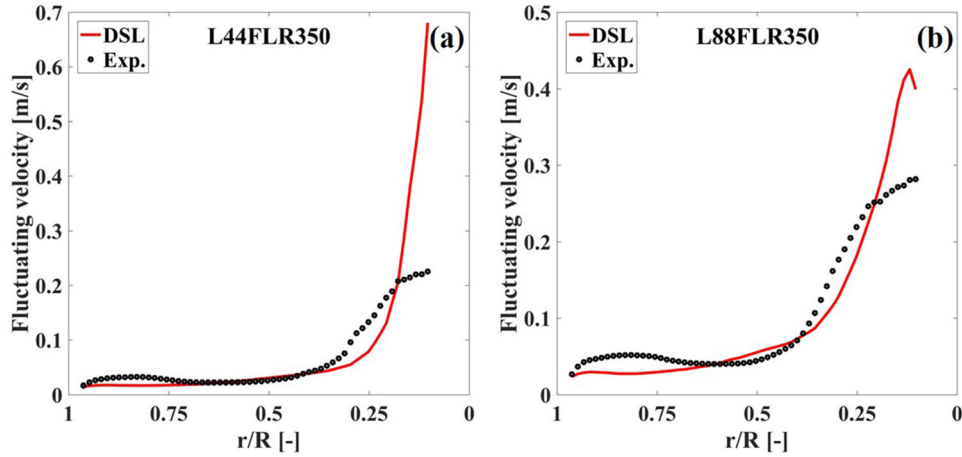
Fig. 5. Velocity fluctuation along the line through the recirculation center: (a) L44FLR350; (b) L88FLR350 (r: radial distance from the axial line; R: radial distance between the axial line.
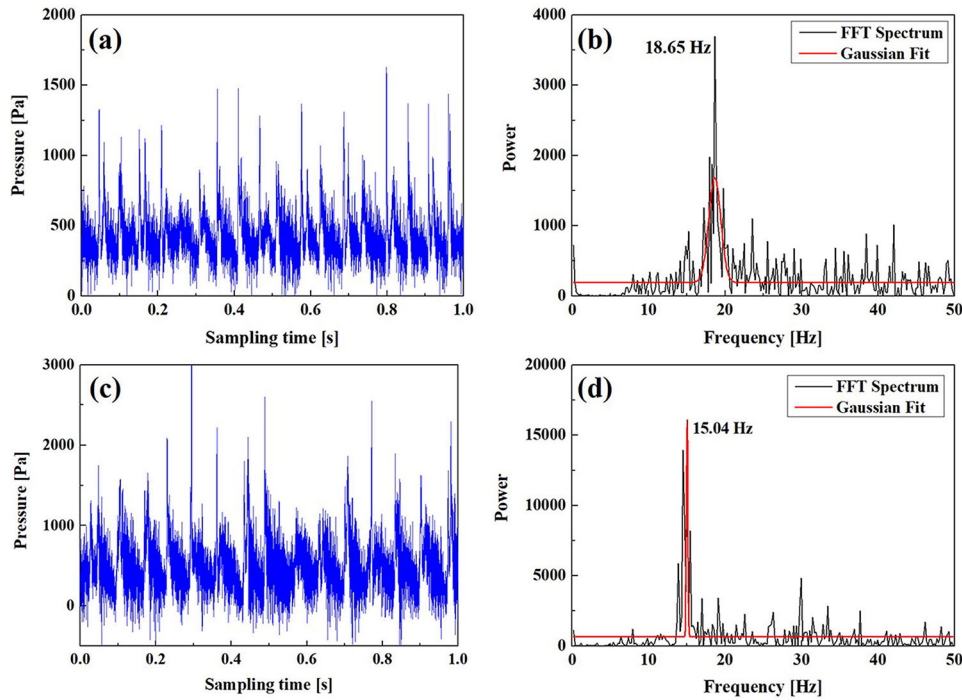

Fig. 6. Pressure signals and bubbling frequencies: (a) and (b) L44FLR350 case; (c) and (d) L44FLR1240 case.

in the above studies is listed in Table S2 (see Supplementary Material). Studies have demonstrated that decreasing surface tension can result in an increase of bubbling frequency.[33,34] The surface tension in the present study is 0.026 N/m, which is much smaller than that in the aforementioned work. This can also partly explain the difference in bubbling frequency between the present results and the results of Gosset et al.[12] and Akashi et al.[13] To compare the bubbling frequency at various conditions, a dimensionless correlation between St number (St = fd_{in}/u_g) and We/Bo was adopted in previous studies,[12,13] where f indicates the bubbling frequency. A similar correlation is

obtained for the present study (see Eq. 7). However, a large deviation of pre-exponential factor and exponent is clearly observed compared to the correlation formulated by Akashi et al.[13] (see Eq. 8). It is worth mentioning that the correlation from the work of Akashi et al. was obtained for the top submerged lance case. The linear relationship can be seen in Fig. S1 (see Supplementary Material). According to Eqs. 3, 5, and 6, the We/Bo equals Fr_m that is the ratio of inertial force to buoyancy force. Apparently, the viscous force and surface tension, which are two major contributing forces influencing the bubble formation,[35,36] are excluded in this correlation. To solve this issue, a new dimensionless
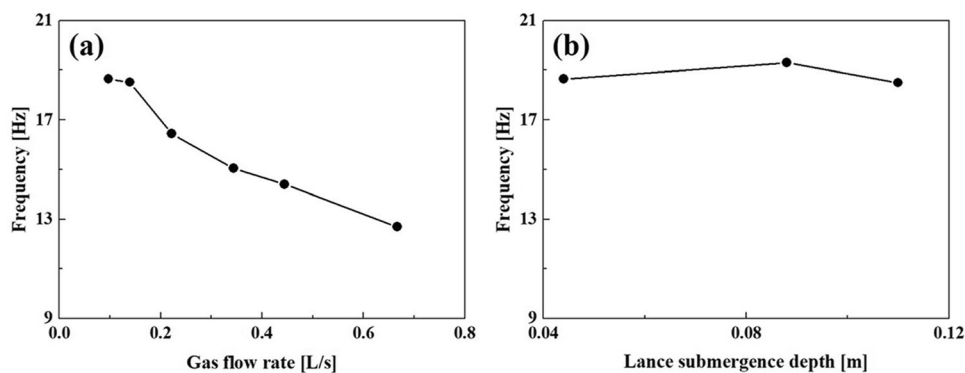
Fig. 7. (a) Bubbling frequency versus gas flow rate (lance submergence depth: 0.044 m); (b) bubbling frequency versus lance submergence depth (gas flow rate: 0.097 L/s).
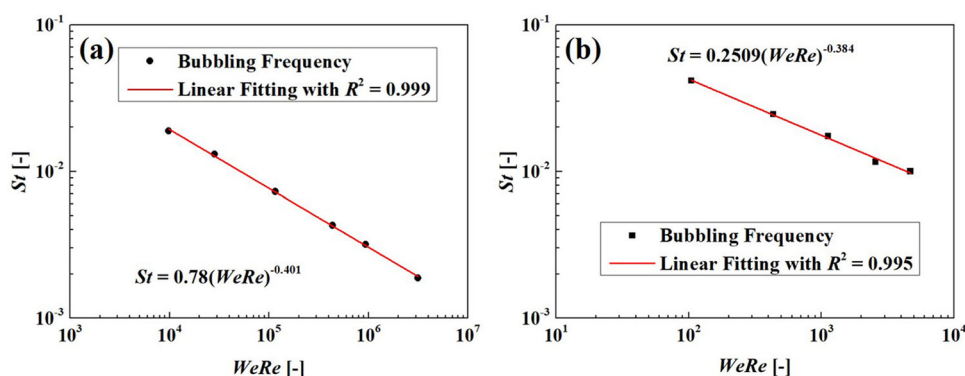

Fig. 8. Proposed dimensionless correlation of (a) the present work and (b) the work of Akashi et al.[13]

correlation is proposed in this work, considering the inertial force, viscous and surface tension. For a comparison, the bubbling frequency measured at the top position in the work of Akashi et al.[13] is also analyzed with the new correlation. The operational parameters in the present work and the work of Akashi et al. are listed in Table S3 (see Supplementary Material). The correlations for this work and the work of Akashi et al. are expressed in Eqs. 9 and 10, and the bubbling frequencies are displayed in Fig. 8. By considering the viscous force and surface tension in the proposed correlation, the deviation of the pre-exponential factor and the exponent is greatly reduced, especially the exponent value, which only has 4.4% difference. The comparisons between the two studies highlight the importance of the viscous force and surface tension on the bubble formation behavior. In this work, the datasets being considered were fitted separately. By comparing the deviation of the pre-exponential factor and exponent of the resulting correlation, the validity of the proposed dimensionless correlation has been evaluated. Both datasets were fitted together with a fitting goodness of 0.90 (see Fig. S2 in Supplementary material), resulting in a correlation with different pre-exponential factor and exponent. To obtain a more convincing correlation by fitting all datasets together, more data from diverse

operational conditions are required. Further experimental and numerical works with different operational systems and conditions are necessary.

$$St = 0.0157(We/Bo)^{-0.602} \tag{7}$$

$$St = 0.00047(We/Bo)^{-0.846} \tag{8}$$

$$St = 0.78(WeRe)^{-0.401} \tag{9}$$

$$St = 0.2509(WeRe)^{-0.384} \tag{10}$$

Surface Sloshing

The volume fraction of liquid phase was monitored at the gas–liquid interface during simulation. Processing the obtained data with FFT technique can identify the frequency of the sloshing wave. Since the application of FFT method was demonstrated in the above section, it will not be repeated here. As seen in Fig. 9, the frequency of the sloshing wave ranges from 2.89 to 3.67 Hz, and it increases with the gas flow rate (Fig. 9a). Increasing the gas flow rate results in an increase in the bubble
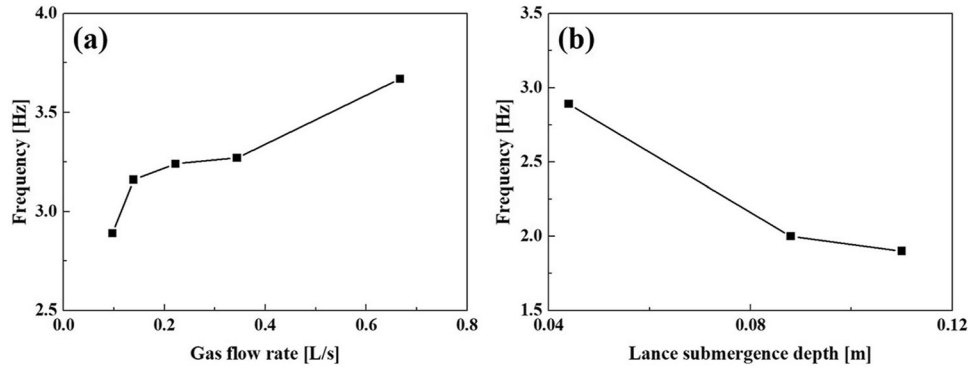
Fig. 9. (a) Sloshing wave frequency versus gas flow rate (lance submergence depth: 0.044 m); (b) sloshing wave frequency versus lance submergence depth (gas flow rate: 0.097 L/s).

diameter, which has been reported by other work,[12,13] and can also be confirmed by the finding in this work that the bubbling frequency decreases with increasing gas flow rate. Large gas bubbles generate a large buoyancy force, which aggravates the surface undulation. Hence, the wave frequency of the surface sloshing is increased. In contrast to the gas flow rate, increasing lance submergence depth leads to decreasing wave frequency (see Fig. 9b). This is due to the drag effect posed by viscous force on gas bubbles rising in the viscous liquid. A reducing influence of the lance submergence depth on the wave frequency is noted as the lance submergence depth further increases.

SUMMARY AND CONCLUSION

The bubble formation and surface sloshing in a TSL flow with a viscous liquid were investigated by means of numerical simulations. To guarantee the accuracy of the numerical model, a detailed validation by HR-PIV experiments was performed in the first place. Subsequently, the numerical model was used to study the influences of gas flow rate and lance submergence depth on the bubble formation and surface sloshing. The key outcomes are summarized as follows:

I.   Numerical results obtained from the coupling model, i.e., VOF-LES-DSL, agree with the HR-PIV experimental data in terms of flow pattern, velocity field, and velocity fluctuation in most of the measured region. The deviations in the near lance region (r/R < 0.25) are caused by the gas phase, which is confirmed by the agreement between the filtered velocity and experimental velocity. The turbulence model, i.e., LES-DSL, fails to predict the velocity fluctuation in the bubbly region (r/R < 0.25), which may be due to the absence of bubble-induced turbulence in this single-phase model. Based on the overall comparison, the numerical model is validated.
II. With the aid of FFT technique, the bubbling frequencies are detected at different gas flow rates, showing a decreasing trend with increasing gas flow rate. This finding is consistent with the experimental observation in the literature. The results show that the lance submergence depth has limited influence on the bubbling frequency. In addition, a new dimensionless correlation (namely, St versus WeRe) is proposed to include the influences of viscous force and surface tension on bubble formation. It turns out that this new correlation has much smaller deviation of the pre-exponential factor and exponent by comparing the present and experimental results from the literature. With this proposed dimensionless correlation, it is possible to evaluate bubbly frequencies obtained at diverse conditions.
III. The wave frequency of surface sloshing increases with increasing gas flow rate, while it decreases with increasing lance submergence depth. The former is caused by the enhanced buoyancy force posed by the enlarging gas bubbles. The latter is mainly due to the viscous drag force, which dissipates the interphase momentum transfer.

SUPPLEMENTARY INFORMATION

The online version contains supplementary material available at https://doi.org/10.1007/s11837-022-05539-y.

CONFLICT OF INTEREST

The authors declare no conflicts of interest.

REFERENCES

1. C. Hagelüken, *Erzmetall* 59, 152. (2006).
2. G.R. Alvear Flores, S. Nikolic, and P.J. Mackey, *JOM* 66, 823. (2014).
3. S. Hughes, *JOM* 50, 30. (2000).
4. P. Mackey, and R. Campos, *Can. Metall. Q.* 40, 355. (2001).
5. J.M. Floyd, *Metall. Mater. Trans. B* 36, 557. (2005).
6. M.L. Bakker, S. Nikolic, and G.R.F. Alvear, *JOM* 63, 60. (2011).
7. M. Kühn, P. Drissen, H. Schrey, in Paper presented at the 2nd European Slag Conference, Düsseldorf, Germany (2000).
8. D. Durinck, F. Engström, S. Arnout, J. Heulens, P.T. Jones, B. Björkman, B. Blanpain, and P. Wollants, *Resour. Conserv. Recycl.* 52, 1121. (2008).
9. Y. Wang, L. Cao, M. Vanierschot, B. Blanpain, and M. Guo, *Metall. Mater. Trans. B* 50, 2354. (2019).
10. Y. Wang, L. Cao, Z. Cheng, B. Blanpain, and M. Guo, *Metall. Mater. Trans. B* 51, 2147. (2020).
11. M.A. Reuter, *Waste Biomass Valor.* 2, 183. (2011).
12. A. Gosset, P. Rambaud, P. Planquart, J.-M. Buchlin, E. Robert, in The 6th International Symposium on Multiphase Flow, Heat Mass Transfer and Energy Conversion, ed by L. Guo (2010), pp. 205–210.
13. M. Akashi, O. Keplinger, N. Shevchenko, S. Anders, M.A. Reuter, and S. Eckert, *Metall. Mater. Trans. B* 51, 124. (2020).
14. Y. Wang, M. Vanierschot, L. Cao, Z. Cheng, B. Blanpain, and M. Guo, *Chem. Eng. Sci.* 192, 1091. (2018).
15. D. Obiso, M. Akashi, S. Kriebitzsch, B. Meyer, M. Reuter, S. Eckert, and A. Richter, *Metall. Mater. Trans. B* 51, 1509. (2020).
16. D. Obiso, M. Reuter, and A. Richter, *Metall. Mater. Trans. B* 52, 2386. (2021).
17. S. Neven, in Department of Materials Engineering (KU Leuven, 2005).
18. A. Kandalam, M. Stelter, M. Reinmöller, M.A. Reuter, A. Charitos, in Proceedings of EMC, p. 249 (2021).
19. P. Liovic, M. Rudman, and J.-L. Liow, *Appl. Math. Model.* 26, 113. (2002).
20. Y. Wang, L. Cao, M. Vanierschot, Z. Cheng, B. Blanpain, and M. Guo, *Chem. Eng. Sci.* 212, 115359. (2020).
21. D. Obiso, M. Reuter, and A. Richter, *Metall. Mater. Trans. B* 52, 3064. (2021).
22. J.-L. Liow, W.H.R. Dickinson, M.J. Allan, and N.B. Gray, *Metall. Mater. Trans. B* 26, 887. (1995).
23. J.-L. Liow, and N.B. Gray, *MetalL Trans. B* 21, 987. (1990).
24. R.L. Player, in The Howard Worner International Symposium on Injection in Pyrometallurgy (TMS, 1996), pp. 439–446.
25. N. Huda, J. Naser, G. Brooks, M.A. Reuter, and R.W. Matusewicz, *Metall. Mater. Trans. B* 43, 39. (2012).
26. M. Vanierschot, T.A.J. Verrijssen, S. Van Buggenhout, M. Hendrickx, and E. Van den Bulck, *Chem. Eng. Sci.* 113, 88. (2014).
27. D.L. Youngs, *Numer. Methods Fluid Dyn.* 24, 273. (1982).
28. J.U. Brackbill, D.B. Kothe, and C. Zemach, *J. Comput. Phys.* 100, 335. (1992).
29. M. Germano, U. Piomelli, P. Moin, and W.H. Cabot, *Phys. Fluids A* 3, 1760. (1991).
30. D.K. Lilly, *Phys. Fluids A* 4, 633. (1992).
31. J.P. Van Doormaal, and G.D. Raithby, *Numer. Heat Transfer* 7, 147. (1984).
32. D. Obiso, S. Kriebitzsch, M. Reuter, and B. Meyer, *Metall. Mater. Trans. B* 50, 2403. (2019).
33. K. Loubière, and G. Hébrard, *Chem. Eng. Process.* 43, 1361. (2004).
34. P. Hanafizadeh, J. Eshraghi, E. Kosari, and W.H. Ahmed, *Part. Sci. Technol.* 33, 645. (2015).
35. M. Jamialahmadi, M.R. Zehtaban, H. Müller-Steinhagen, A. Sarrafi, and J.M. Smith, *Chem. Eng. Res. Des.* 79, 523. (2001).
36. G.-Q. Chen, X. Huang, A.-M. Zhang, and S.-P. Wang, *Phys. Fluids* 31, 027102. (2019).